JOURNAL OF SOLID STATE CHEMISTRY 73, 362–380 (1988)

# A Neutron Diffraction Study of Hydrogen Positions at 13 K, Domain Model, and Chemical Composition of Staurolite*

K. STÅHL

*Inorganic Chemistry 2, University of Lund, P.O.B. 124, S-22100 Lund, Sweden*

Å. KVICK

*Chemistry Department, Brookhaven National Laboratory, Upton, New York 11973*

AND J. V. SMITH

*Geophysical Sciences and Materials Research Laboratory, The University of Chicago, Chicago, Illinois 60637*

Received June 1, 1987

Comparison of new neutron and old X-ray diffraction data for single crystals of staurolite from Pizzo Forno yielded unique answers to some, but not all, outstanding structural questions. Neutron data were collected at 13(1) K for a crystal with assumed composition $Li_{0.07}Mg_{0.87}Ti_{0.14}V_{0.01}Cr_{0.01}Mn_{0.04}Fe^{2+}_{3.00}Fe^{3+}_{0.06}Co_{0.01}Zn_{0.05}Al_{17.69}Si_{7.67}O_{48}H_{3.41}F_{0.01}$, $M_w = 1671$, $a = 7.8639(10)$, $b = 16.625(2)$, $c = 5.651(2)$ Å, $\beta = 90.015(14)°$, $C2/m$, $Z = 1$, $D_x = 3.75$ g cm$^{-3}$; 1874 (1024 unique) reflections, $\lambda = 1.1598(1)$ Å, $R(F) = 3.3\%$. The diffraction evidence is consistent with full occupancy of the Si, Al(1), Al(2), and Al(3) sites, but not of the other ones. Detailed assignment of atoms is based on diffraction evidence and crystal-chemical arguments, but some uncertainties remain; thus exchange of (Li + Fe) by two Mg would have little effect on diffraction data. A structural model with three types of domains is proposed: ~63% type 1, (Fe, etc.) + H(1); ~22% type 2, (Mg, etc.) + H(2); ~15% type 3, (Fe, etc.) without hydrogen.

For the orthorhombic pseudostructure, the occupancies of the two hydrogen sites place strong restrictions on the other site occupancies. The 25(4)% observed occupancy of H(2) limits the occupancy of the nearby (Fe, etc.) site to a maximum of 75(4)%. To explain the neutron scattering, the Fe site must be occupied mainly by Fe; Li, Mn, Zn, and Mg may also occupy this site. A good ionic balance is attained for the type 2 domain if the U site from the old X-ray work is occupied simultaneously with H(2). To match the neutron data, assignment of 21(2)% Mg to the U site is plausible, but other substituents are possible. H(2) lies directly between two O(1) atoms at ~0.9 and 2.3 Å, and H(1) is displaced away from the Fe site so that it is bonded to one O(1) at 1.01 Å and one O(3) at 2.07 Å. Four-fifths of the Fe atoms should be displaced from $z = 0.25$ because of electrostatic repulsion from H(1), and one-fifth should not be. This is consistent with the threefold distortion of the electron-density peak for the Fe site and the intensity ratio for the doublets in the Mössbauer spectrum. Assignment of 0.3 Al to the eight Si sites explains the low neutron scattering. Some Mg atoms, together with Ti and $Fe^{3+}$ ones, are placed in the Al sites, but assignments among the three sites are uncertain. A plausible

* Research performed at Brookhaven National Laboratory under Contract DE-AC02-76CH00016 with the U. S. Department of Energy and supported by its Division of Chemical Sciences, Office of Basic Energy Sciences.

0022-4596/88 $3.00

structural formula is: $[Si\ 7.67, Al\ 0.33]_8[Fe^{2+}\ 3.00, Li\ 0.07, Mn\ 0.04, Zn\ 0.02, Co\ 0.01]_{3.14}$[Al(1) site: Al 7.94, $Fe^{3+}$ $0.06]_8$[Al(2) site: Al 7.52, Mg 0.35, Ti 0.11, V 0.01, Cr $0.01]_8$[Al(3) site: Al 1.88, Mg 0.09, Ti $0.03]_2$[U site: Mg 0.41, Zn $0.02]_{0.43}[H(1)]_{2.54}[H(2)]_{0.86}$. For the monoclinic structure, the A and B subcomponents are less different for the crystal used for neutron diffraction than for the smaller one used for X-ray diffraction. Maximum deviation from the orthorhombic superstructure would be generated by the following occupancies: Al(3A) 100%, H(1A) 63%, H(2A) and Mg(A) 22%. Atoms essentially unaffected by chemical substitutions have displacement factors consistent with zero-point motions, but some (especially Fe, O(1), O(3), H(2)) have large B values indicative of more than one center-of-motion. All bond lengths and angles are reasonable when chemical substitutions are considered. 

## Introduction

Staurolite has complex crystallographic and crystal-chemical properties which are gradually being resolved by application of modern analytical techniques (see reviews in (*1*, *2*)). The concept of alternating kyanite and Fe–Al–hydroxide layers (*3*) remains a reasonable first approximation, but (a) the symmetry was lowered from *Ccmm* to *C*2/*m* (*4–6*), (b) the subunits with the *topology* of kyanite and Fe–Al–hydroxide contain minor but important chemical substitutions from the ideal formulas (*6*), (c) additional weakly occupied octahedral sites are present in a specimen from Pizzo Forno in the St. Gotthard region (*6*) but were not reported for a Zn-rich specimen (*7*), and (d) there may be submicroscopic twins (*6*), or antiphase domain boundaries (*8*).

The long-standing uncertainty about the number of hydrogen atoms per unit cell (*1*, *9*, *10*) was resolved by modern gravimetric analyses (*11*, *12*) coupled with ion microprobe analyses (*12*). Those staurolites which coexist with garnet and biotite contain 2.7–3.4 H per unit cell, whereas those which formed under more oxidizing conditions contain 4.1–4.2 H. The specimens used in all recent diffraction studies belong to the first group.

Two hydrogen positions, both associated with the undersaturated O(1) atom (*7*), were located with low precision by combining information from two-dimensional neutron diffraction and nuclear magnetic resonance (*13*). A third set of broad resonances was unassigned. The two hydrogen positions were located accurately by three-dimensional neutron diffraction from a St. Gotthard specimen at 100 K (*14*).

Because staurolite crystals commonly incorporate mechanical impurities during growth and subsequently become altered, bulk chemical analyses must be regarded with caution. Electron and ion microprobe techniques can get around these problems, but calibration is subject to unknown systematic errors. The latest compilation of careful analyses (*15*) reports 13 elements (including Li) at concentrations above 0.01 wt%; electron microprobe analyses for Fe and Al were arbitrarily multiplied by 1.04 and 0.987 to reduce discrepancies with other analyses. Interpretation of the structural and chemical state of Fe is difficult, but it is certain from spectroscopic measurements (Mössbauer (*6*, *13*, *16–21*), near-edge X-ray absorption (*22*), VUV (*17*)) that most Fe is divalent in tetrahedral coordination. The color of staurolite is proportional to the Ti content, and was attributed to charge transfer between Fe and Ti in adjacent tetrahedral sites (*23*).

The present three-dimensional neutron diffraction study of staurolite from the same rock specimen used in an X-ray study (*6*) was undertaken to (a) precisely locate the H atoms and (b) use the differences in X-ray and neutron scattering factors to further constrain the assignment of atoms to the structural sites. Data were collected at

13 K to take advantage of the smaller thermal motions than for the X-ray study at room temperature.

## Experimental

A gem-quality ruby crystal from a kyanite–staurolite–mica schist from the St. Gotthard region, Switzerland (University of Chicago Mineralogy Collection, 1558), was mounted on a four-circle diffractometer at the Brookhaven National Laboratory High Flux Beam Reactor and cooled to 13(1) K with a DISPLEX CS-202 refrigerator (Air Products and Chemicals, Inc.). Neutrons of wavelength 1.1598(1) Å were obtained with a Ge (220) monochromator calibrated by least-squares fit of 32 sin $2\theta$ values from a KBr crystal at 298 K ($a_0$ = 6.6000(1) Å): all errors were given as standard deviations in brackets to the same decimal level. The cell dimensions in the abstract were obtained by least-squares fit of 63 sin $2\theta$ values between 44 and 69°. These cell dimensions at 13 K are within $2\sigma$ of those obtained by X-ray powder diffractometry at room temperature (*6*), and the thermal expansion coefficients ($a$ = +0.09(4)%, $b$ = −0.03(3), $c$ = +0.09(5), $V$ = 0.15(12)) are small in accord with the close-packed nature of the crystal structure.

The electron microprobe analysis in (*6*) is similar to that of specimen PF-2 in (*15*), and the cell dimensions in (*6*) and (*15*) agree at the $1\sigma$ level. Hence it was decided to use the preferred chemical analysis in (*15*) which gives the following numbers of atoms per 48 oxygen atoms per unit cell when 2% of the iron is arbitrarily assumed to be trivalent: Si 7.668, Al 17.686, Ti 0.138, Cr 0.011, V 0.009, $Fe^{3+}$ 0.061, $Fe^{2+}$ 3.002, Co 0.007, Mg 0.886, Mn 0.042, Zn 0.047,Li 0.067, H 3.408, F 0.009 (caution: see (*15*) for discussion of error). The analyses correspond to $M_w$ = 1671 and $D_x$ = 3.75 g cm$^{-3}$.

A total of 2190 reflections was collected with sin $\theta/\lambda \leq 0.706$ Å$^{-1}$ and $0 < h < 11$, $-22 < k < 23$, $-7 < l < 7$, using $\omega/2\theta$ step scans ($\Delta 2\theta$ = 3.2° for $2\theta < 60°$ and 1.5(1 + 2.05 tan $\theta$) for 60° to 113°). The background was taken as 5 times the sum of the first and last tenth of a scan. Lorentz and absorption corrections were made with a 6 × 6 × 6 Gaussian grid. For the prismatic crystal (1.2 × 1.9 × 2.8 mm = 4.6 mm$^3$; {010}, {110}, and {001}), the absorption coefficient of 0.24 cm$^{-1}$ gave transmission factors of 0.96–0.98.

Because of the strong orthorhombic pseudosymmetry, two choices of origin at a center of symmetry give similar atomic coordinates. In an abstract (*24*), we reported a set of coordinates for a different origin than that used in (*6*). Table I contains coordinates transformed by $z_1 = z_2 + 0.5$ to match those in Table II of (*6*).

Difference Fourier maps revealed four H positions of which the pair H(1A) and H(1B) correspond to those in (*13*, *14*). Figure 1a shows a map in which the broad elongated peaks of negative scattering for H(2A) and H(2B) are compared with the tight round peaks for Mg(1) and Mg(2); all other atoms were included in $F_c$. Figure 1b shows that addition of anisotropic displacement parameters for H(2A) and H(2B) produces a satisfactory difference map with residual density only around the Fe site.

Two standard reflections monitored every 50 measured reflections showed a 3.5% intensity increase after fuel reloading, and two scale factors were used. One isotropic extinction parameter, 0.27(2) × 10$^4$ (type I, Lorentzian mosaicity (*25*)) was refined in the initial least-squares cycles, but then kept constant. Twenty-nine reflections with extinction correction factors (on $F_o^2$) > 1.25 were given zero weight in the final cycles together with 140 weak reflections with $F_o^2/F_c^2 > 5$, which were assumed to be affected by multiple scattering. Anisotropic displacement parameters were used for all atoms giving a total with the occupancy fac-

TABLE I

ATOMIC COORDINATES, POPULATION FACTORS, AND ISOTROPIC DISPLACEMENT PARAMETERS FOR STAUROLITE AT 13 K

| Atom | $x$ | $y$ | $z$ | Population | $B_{iso}$ (Å$^2$) |
|---|---|---|---|---|---|
| Fe | 0.39411(8) | 0.0 | 0.24925(12) | 4 × 0.732(4) | 1.01(2) |
| Si | 0.13424(8) | 0.16611(3) | 0.24949(12) | 8 × 0.990(6) | 0.29(2) |
| Al(1A) | 0.5 | 0.17516(6) | 0 | 4 × 1.006(10) | 0.31(3) |
| Al(1B) | 0.5 | 0.17512(6) | 0.5 | 4 × 1.026(10) | 0.36(3) |
| Al(2) | 0.26316(9) | 0.41012(5) | 0.25050(14) | 8 × 0.971(7) | 0.38(2) |
| Al(3A) | 0 | 0 | 0 | 2 × 0.532(12) | 0.24(7) |
| Al(3B) | 0 | 0 | 0.5 | 2 × 0.452(12) | 0.32(8) |
| U(A) | 0.5 | 0 | 0 | 2 × 0.118(8) | 0.41(20) |
| U(B) | 0.5 | 0 | 0.5 | 2 × 0.087(8) | 0.27(26) |
| O(1A) | 0.23504(9) | 0 | 0.96477(16) | 4 × 1 | 0.67(2) |
| O(1B) | 0.23597(9) | 0 | 0.53375(17) | 4 × 1 | 0.68(2) |
| O(2A) | 0.25518(5) | 0.16154(3) | 0.01510(9) | 8 × 1 | 0.39(1) |
| O(2B) | 0.25489(5) | 0.16143(3) | 0.48471(9) | 8 × 1 | 0.40(1) |
| O(3) | 0.00190(6) | 0.08887(3) | 0.24858(9) | 8 × 1 | 0.61(1) |
| O(4) | 0.02107(7) | 0.24924(3) | 0.25000(9) | 8 × 1 | 0.40(1) |
| O(5) | 0.52685(6) | 0.10014(3) | 0.24973(9) | 8 × 1 | 0.43(1) |
| H(1A) | 0.1264(5) | 0 | 0.4406(9) | 4 × 0.380(12) | 1.84(11) |
| H(1B) | 0.1259(7) | 0 | 0.0587(13) | 4 × 0.284(16) | 1.51(15) |
| H(2A) | 0.2495(45) | 0 | 0.3801(37) | 4 × 0.116(16) | 4.5(9) |
| H(2B) | 0.2433(94) | 0 | 0.1235(48) | 4 × 0.130(24) | 8.6(2.3) |

*Note*. Population given as full occupancy multiplied by fractional occupancy obtained by assuming occupancy by the atom in the first column. $B_{iso} = 4\Sigma_i\Sigma_j\beta_{ij}(a_i \cdot a_j)/3$. The populations are based on the assumption that the site is fully occupied by the listed element; for the U site, Mg is assumed. See text for uncertainties in occupation.

TABLE II

ANISOTROPIC TEMPERATURE FACTORS (×10$^2$) OF STAUROLITE AT 13 K

| | $\beta_{11}$ | $\beta_{22}$ | $\beta_{33}$ | $\beta_{12}$ | $\beta_{13}$ | $\beta_{23}$ |
|---|---|---|---|---|---|---|
| Fe | 0.455(11) | 0.017(2) | 1.345(25) | 0 | −0.073(10) | 0 |
| Si | 0.079(10) | 0.015(2) | 0.394(22) | 0.000(3) | −0.069(9) | −0.004(4) |
| Al(1A) | 0.069(17) | 0.025(4) | 0.378(36) | 0 | −0.062(14) | 0 |
| Al(1B) | 0.102(17) | 0.031(4) | 0.387(36) | 0 | −0.060(14) | 0 |
| Al(2) | 0.101(13) | 0.015(3) | 0.570(29) | −0.009(3) | −0.071(11) | 0.001(5) |
| Al(3A) | 0.038(51) | 0.007(10) | 0.43(10) | 0 | 0.041(36) | 0 |
| Al(3B) | 0.062(64) | 0.003(12) | 0.59(12) | 0 | −0.165(44) | 0 |
| U(A) | 0.16(14) | 0.033(30) | 0.36(28) | 0 | 0.01(10) | 0 |
| U(B) | 0.24(19) | 0.007(38) | 0.12(35) | 0 | −0.12(14) | 0 |
| O(1A) | 0.297(11) | 0.023(2) | 0.798(27) | 0 | −0.002(11) | 0 |
| O(1B) | 0.307(11) | 0.023(3) | 0.814(29) | 0 | −0.144(11) | 0 |
| O(2A) | 0.119(8) | 0.031(2) | 0.429(17) | 0.000(2) | −0.050(8) | −0.009(3) |
| O(2B) | 0.125(8) | 0.031(2) | 0.434(17) | 0.001(2) | −0.056(8) | 0.010(3) |
| O(3) | 0.127(8) | 0.035(2) | 0.888(17) | −0.001(2) | −0.060(7) | 0.003(3) |
| O(4) | 0.145(8) | 0.024(2) | 0.454(16) | 0.009(2) | −0.060(7) | 0.000(3) |
| O(5) | 0.118(8) | 0.033(2) | 0.485(16) | −0.006(2) | −0.071(7) | 0.004(3) |
| H(1A) | 0.51(9) | 0.200(16) | 1.60(15) | 0 | −0.41(7) | 0 |
| H(1B) | 0.44(12) | 0.177(20) | 1.16(20) | 0 | 0.22(8) | 0 |
| H(2A) | 4.2(1.0) | 0.14(6) | 1.1(8) | 0 | −0.6(5) | 0 |
| H(2B) | 8.9(2.8) | 0.14(7) | 1.8(1.0) | 0 | 1.2(10) | 0 |

*Note*. The temperature factor is given by exp $-\beta_{ij}h_ih_j$.

tors of 146 parameters refined with 1874 (1024 unique) reflections in the final cycles. All values of (parameter shift/parameter e.s.d.) were <0.1. The full-matrix least-squares refinement minimized $\Sigma w(F_o^2 - F_c^2)^2$ with final $w^{-1} = (\sigma_c(F^2))^2 + (0.05\,F^2)^2 + 0.04$ and $\sigma(F^2)$ from counting statistics. Final $R$-factors were $R(F^2) = 0.055$ (0.087 including zero weighted reflections), $R(F) = 0.033$, $R_w(F^2) = 0.077$, and $S = 1.25$. The highest residual peak in the final difference Fourier map corresponds to 2.3% of an oxygen atom. The internal agreement factor $R_{int}(F^2)$ for 846 reflections of types $(hkl)$, $(hk\bar{l})$, and $(h\bar{k}\bar{l})$ after extinction correction is 0.041.

Neutron scattering lengths for the site labels in Table I were taken from (*26*), and the computer programs from (*27*).[1]

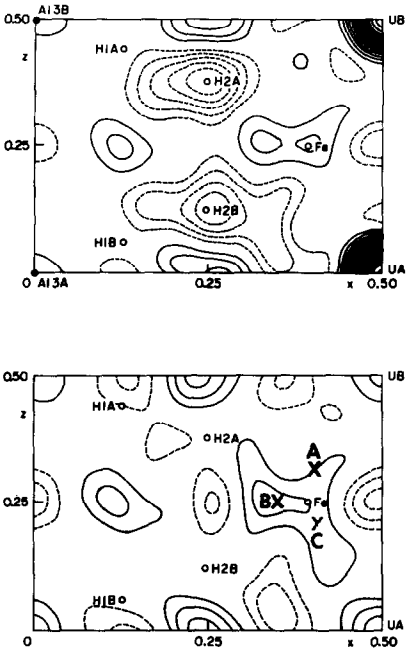


FIG. 1. Difference Fourier maps at $y = 0$, without (a) and with (b) inclusion in $F_c$ of U(A), U(B), H(2A), and H(2B). Crosses A, B, and C correspond to the difference Fourier peaks found for the Fe atom from X-ray diffraction analysis at room temperature (Ref. (*6*)). Continuous and dashed lines, respectively, show positive and negative scattering density.

## Discussion

It is necessary to distinguish clearly between the unambiguous experimental evidence on the geometrical properties of the staurolite structure, and the plausible but speculative ideas on the structural disorder and the chemical substitutions. For some of the discussion, it is sufficient to consider the idealized site occupancies in Table I, but complex chemical substitutions and site displacements must be considered for interpretation of the anisotropic "temperature" factors (Table II) and the selected distances and angles (Table III). For reasons discussed later, the U sites of uncertain occupancy from the old X-ray data are now thought to contain more Mg than other possible substituents. For convenience, the U designation is retained, but occupancy by Mg is assumed in much of the paper to simplify discussion.

### *General Features of the Crystal Structure*

The unit cell of staurolite contains 48 oxygen atoms in the topology of cubic closest packing. To a first approximation, the structure consists of slabs of $Al(VI)_8Si(IV)_4O_{20}$ (kyanite) alternating with layers of $Al(VI)_{0.7}Fe^2(IV)_2O_2(OH)_2$ along $b$ (Fig. 1 of Ref. (*1*)). However, an X-ray structure determination (*6*) demonstrated that there were complex cation substitutions which would require further study. It will now be demonstrated from a combined consideration of all the available experimental data plus theoretical crystal-chemical arguments that the present staurolite appears to be an ensemble of six principal types of structural domains. Each type contains a cation distribution which gives a good charge balance for a simple ionic model. The six types consist of three pairs (labeled *1*, *2*, and *3*) and

[1] Copies of supplementary materials may be obtained directly from the authors.

TABLE III

SELECTED DISTANCES (Å) AND ANGLES (°) IN STAUROLITE AT 13 K

| | | | |
|---|---|---|---|
| Fe–O(1A) | 2.0372(12) | O(1A)–Fe–O(1B) | 104.39(4) |
| Fe–O(1B) | 2.0323(12) | O(1A)–Fe–O(5) | 109.11(3) |
| 2 Fe–O(5) | 1.9649(7) | O(1B)–Fe–O(5) | 108.90(3) |
| Mean | 1.9998 | O(5) –Fe–O(5) | 115.82(4) |
| Fe–H(1B) | 2.369(7) | Fe–Mg(A) | 1.6361(8) |
| Fe–H(1A) | 2.367(5) | Fe–Mg(B) | 1.6437(8) |
| Fe–H(2B) | 1.38(7) | Fe–H(2A) | 1.36(3) |
| | | | |
| Si–O(2A) | 1.6322(9) | O(2A)–Si–O(2B) | 108.63(5) |
| Si–O(2B) | 1.6352(9) | O(2A)–Si–O(3) | 109.15(4) |
| Si–O(3) | 1.6529(8) | O(2A)–Si–O(4) | 110.85(4) |
| Si–O(4) | 1.6437(8) | O(2B)–Si–O(3) | 109.33(4) |
| Mean | 1.6410 | O(2B)–Si–O(4) | 110.66(4) |
| | | O(3) –Si–O(4) | 108.19(4) |
| | | | |
| 2 Al(1A)–O(2A) | 1.9404(5) | 2 Al(1B)–O(2B) | 1.9428(4) |
| 2 Al(1A)–O(4) | 1.8982(9) | 2 Al(1B)–O(4) | 1.8986(9) |
| 2 Al(1A)–O(5) | 1.8952(9) | 2 Al(1B)–O(5) | 1.8969(9) |
| Mean | 1.9113 | Mean | 1.9128 |
| | | | |
| O(2A)–Al(1A)–O(2A) | 166.59(7) | O(2B)–Al(1B)–O(2B) | 166.55(7) |
| O(2A)–Al(1A)–O(4) | 91.33(3) | O(2B)–Al(1B)–O(4) | 91.39(3) |
| O(2A)–Al(1A)–O(4) | 97.55(3) | O(2B)–Al(1B)–O(4) | 97.52(3) |
| O(2A)–Al(1A)–O(5) | 81.09(3) | O(2B)–Al(1B)–O(5) | 81.14(3) |
| O(2A)–Al(1A)–O(5) | 90.07(3) | O(2B)–Al(1B)–O(5) | 90.01(3) |
| O(4) –Al(1A)–O(4) | 97.07(6) | O(4) –Al(1B)–O(4) | 97.04(6) |
| O(4) –Al(1A)–O(5) | 178.60(2) | O(4) –Al(1B)–O(5) | 178.59(2) |
| O(4) –Al(1A)–O(5) | 82.63(3) | O(4) –Al(1B)–O(5) | 82.58(3) |
| O(5) –Al(1A)–O(5) | 97.69(6) | O(5) –Al(1B)–O(5) | 97.69(6) |
| | | | |
| H(1B)–O(1A) | 1.009(5) | O(1A)–U(A)–O(1A) | 180 |
| 2 H(1B)–O(3) | 2.070(4) | O(1A)–U(A)–O(5) | 99.05(2) |
| 2 O(1A)–O(3) | 2.849(1) | O(1A)–U(A)–O(5) | 80.95(2) |
| O(1A)–H(1A)–O(3) | 132.3(2) | O(5) –U(A)–O(5) | 81.21(3) |
| O(3) –H(1A)–O(3) | 91.1(2) | O(5) –U(A)–O(5) | 98.79(3) |
| | | O(5) –U(A)–O(5) | 180 |
| H(2A)–O(1B) | 0.88(2) | | |
| H(2A)–O(1A) | 2.35(2) | | |
| O(1A)–O(1B) | 3.215(2) | | |
| O(1A)–H(2A)–O(1B) | 170(3) | | |
| | | | |
| Al(2)–O(1A) | 1.9269(10) | O(1A)–Al(2)–O(1B) | 78.36(5) |
| Al(2)–O(1B) | 1.9285(10) | O(1A)–Al(2)–O(2A) | 89.32(4) |
| Al(2)–O(2A) | 1.9216(10) | O(1A)–Al(2)–O(2B) | 167.07(5) |
| Al(2)–O(2B) | 1.9168(10) | O(1A)–Al(2)–O(3) | 88.98(4) |
| Al(2)–O(3) | 1.8775(9) | O(1A)–Al(2)–O(5) | 94.39(5) |
| Al(2)–O(5) | 1.8661(9) | O(1B)–Al(2)–O(2A) | 167.00(5) |
| Mean | 1.9062 | O(1B)–Al(2)–O(2B) | 89.29(4) |
| | | O(1B)–Al(2)–O(3) | 89.60(4) |
| 2 Al(3A)–O(1A) | 1.8590(7) | O(1B)–Al(2)–O(5) | 94.36(5) |
| 4 Al(3A)–O(3) | 2.0387(6) | O(2A)–Al(2)–O(2B) | 102.68(5) |
| Mean | 1.9788(3) | O(2A)–Al(2)–O(3) | 94.37(4) |
| 2 Al(3A)–H(1B) | 1.044(6) | O(2A)–Al(2)–O(5) | 82.34(4) |

TABLE III—*Continued*

| | | | |
|---|---|---|---|
| 2 Al(3A)–H(2B) | 2.04(7) | O(2B)–Al(2)–O(3) | 94.81(4) |
| | | O(2B)–Al(2)–O(5) | 82.62(4) |
| 2 Al(3B)–O(1B) | 1.8655(7) | O(3) –Al(2)–O(5) | 175.25(5) |
| 4 Al(3B)–O(3) | 2.0497(6) | | |
| Mean | 1.9883(3) | O(1A)–Al(3A)–O(1A) | 180 |
| 2 Al(3B)–H(1A) | 1.049(5) | O(1A)–Al(3A)–O(3) | 93.80(3) |
| 2 Al(3B)–H(2A) | 2.08(4) | O(1A)–Al(3A)–O(3) | 86.20(3) |
| | | O(3) –Al(3A)–O(3) | 87.12(4) |
| 2 U(A)–O(1A) | 2.0931(8) | O(3) –Al(3A)–O(3) | 92.88(4) |
| 4 U(A)–O(5) | 2.1926(6) | O(3) –Al(3A)–O(3) | 180 |
| Mean | 2.1594(3) | | |
| U(A)–H(2B) | 2.14(7) | O(1B)–Al(3B)–O(1B) | 180 |
| | | O(1B)–Al(3B)–O(3) | 93.66(3) |
| 2 U(B)–O(1B) | 2.0850(7) | O(1B)–Al(3B)–O(3) | 86.34(3) |
| 4 U(B)–O(5) | 2.1945(5) | O(3) –Al(3B)–O(3) | 87.76(3) |
| Mean | 2.1580(2) | O(3) –Al(3B)–O(3) | 92.24(3) |
| U(B)–H(2A) | 2.08(3) | O(3) –Al(3B)–O(3) | 180 |
| | | | |
| H(2B)–O(1A) | 0.90(3) | O(1B)–U(B)–O(1B) | 180 |
| H(2B)–O(1B) | 2.32(3) | O(1B)–U(B)–O(5) | 98.89(2) |
| O(1A)–O(1B) | 3.215(2) | O(1B)–U(B)–O(5) | 81.11(2) |
| O(1A)–H(2B)–O(1B) | 174(6) | O(5) –U(B)–O(5) | 81.32(3) |
| | | O(5) –U(B)–O(5) | 96.68(3) |
| H(1A)–O(1B) | 1.010(4) | O(5) –U(B)–O(5) | 180 |
| 2 H(1A)–O(3) | 2.078(3) | | |
| 2 O(1B)–O(3) | 2.858(1) | | |
| O(1B)–H(1A)–O(3) | 132.4(1) | | |
| O(3) –H(1A)–O(3) | 90.6(2) | | |

each pair is related geometrically by a $c/2$ translation between the *A* and *B* subtypes. For the ideal mathematical limit in which the *A* and *B* subtypes become identical in both cation type and population, the overall symmetry for a fully disordered arrangement of *A* and *B* is *Ccmm*; when $A \neq B$, the symmetry is $C2/m$.

For clarity, the proposed structural domains are given first in a simplified arrangement (Table IV) in which only $Fe^2$, Si, Al, Mg, and H are assigned to the cation sites. The models were developed from comparison of the distances between adjacent cation sites (Table V), and checked by consideration of the coordination and electrostatic valence balance (Table VI).

Detailed consideration of the chemical composition given in the experimental section, plus the relative ionic radii and the X-ray and neutron scattering factors (Table VII), led to extension of the simple chemical model to the complex one in Table VIII (a) in which there is no $Fe^2$ in the U site and in which site assignments are proposed for the minor elements Ti, Li, Zn, etc. The effects on the population factors for random occupancy of sites by $Fe^2$ and Mg, and for transfer of Mg and Fe between the Fe and U sites are shown in Table VIII (b) and (c). After discussion of the new domain model, it is shown that there are topochemical restrictions at the boundaries between the structural domains.

TABLE IV

SIMPLIFIED OCCUPANCY MODELS

(a) Monoclinic Population Fractions

| Label | Fe | Al(3A) | Al(3B) | Mg(A) | Mg(B) | H(1A) | H(1B) | H(2A) | H(2B) |
|---|---|---|---|---|---|---|---|---|---|
| Wyckoff | 4 | 2 | 2 | 2 | 2 | 4 | 4 | 4 | 4 |
| Observed | 0.732(4) | 0.532(12) | 0.452(12) | 0.118(8) | 0.087(8) | 0.380(12) | 0.284(16) | 0.116(16) | 0.130(24) |
| Model *1A* | 0.365 | 0.365 | | | | 0.365 | | | |
| Model *1B* | 0.27 | | 0.27 | | | | 0.27 | | |
| Model *2A* | | 0.115 | | 0.115 | | | | 0.115 | |
| Model *2B* | | | 0.10 | | 0.10 | | | | 0.10 |
| Model *3A* | 0.06 | 0.06 | | | | | | | |
| Model *3B* | 0.09 | | 0.09 | | | | | | |
| Sum *1A–3B* | 0.785 | 0.54 | 0.46 | 0.115 | 0.10 | 0.365 | 0.27 | 0.115 | 0.10 |

(b) Orthorhombic Population Fractions

| Label | Fe | Al(3) | Mg | H(1) | H(2) |
|---|---|---|---|---|---|
| Wyckoff | 4 | 4 | 4 | 4 | 4 |
| Model *1* | 0.635 | 0.635 | | 0.635 | |
| Model *2* | | 0.215 | 0.215 | | 0.215 |
| Model *3* | 0.15 | 0.15 | | | |
| Sum *1–3* | 0.785 | 1.00 | 0.215 | 0.635 | 0.215 |

*Note.* Mg is occupying the U site in this simplified model.

### *Simplified Occupancy Model*

For reasons to be given in the next section, it was concluded that the Si, Al(1), and Al(2) sites are fully occupied and that the Fe, Al(3), and Mg sites are partly occupied mainly by the designated element. In the initial development of the domain model, it was assumed that the observed population factors would not change

TABLE V

DISTANCES BETWEEN SITES IN $Z = 0$ PLANE

| Label | Unadjusted occupancy | Distance (Å) to listed site | | | | | | | |
|---|---|---|---|---|---|---|---|---|---|
| | | Al(3A) | Al(3B) | Mg(A) | Mg(B) | H(1A) | H(1B) | H(2A) | H(2B) |
| Fe | 0.732(4) | $3.40^{1A}$ | $3.41^{1B}$ | 1.64* | 1.64* | $2.37^{1A}$ | $2.37^{1B}$ | 1.36* | 1.38* |
| Al(3A) | 0.532(12) | 0 | 2.83* | $3.93^{2A}$ | 4.84 | $2.68^{1A}$ | 1.04* | $2.91^{2A}$ | 2.04* |
| Al(3B) | 0.452(12) | | 0 | 4.84 | $3.93^{2B}$ | 1.05* | $2.68^{1B}$ | 2.08* | $2.86^{2B}$ |
| Mg(A) | 0.118(8) | | | 0 | 2.83* | 3.85 | 2.96* | $2.91^{2A}$ | 2.14* |
| Mg(B) | 0.087(8) | | | | 0 | 2.96* | 3.86 | 2.08* | $2.93^{2B}$ |
| H(1A) | 0.380(12) | | | | | 0 | 2.16* | 1.03* | 2.01* |
| H(1B) | 0.284(16) | | | | | | 0 | 2.06* | 0.99* |
| H(2A) | 0.116(16) | | | | | | | 0 | 1.45* |
| H(2B) | 0.130(24) | | | | | | | | 0 |

*Note.* Superscripts 1A–2B refer to distances between occupied sites for models *1A–2B* in Table VI. An asterisk shows a distance which is short for simultaneous occupancy of the pair of sites. Note that Mg is occupying the U site in this simplified model.

TABLE VI

COORDINATION OF OXYGEN ATOMS AROUND CATION SITES (a) AND VALENCE SUMS FOR MODELS 1–3 OF TABLE VI (b)

(a)

| Site | Formal valence | Number of oxygen neighbors and distance (Å) | | | | |
|---|---|---|---|---|---|---|
| | | O(1) | O(2) | O(3) | O(4) | O(5) |
| Fe | 2/4 = 0.5 | 2 × 2.03 | | | | 2 × 1.96 |
| Si | 4/4 = 1.0 | | 2 × 1.63 | 1 × 1.65 | 1 × 1.64 | |
| Al(1) | 3/6 = 0.5 | | 2 × 1.94 | | 2 × 1.90 | 2 × 1.90 |
| Al(2) | 3/6 = 0.5 | 2 × 1.93 | 2 × 1.92 | 1 × 1.88 | | 1 × 1.87 |
| Al(3) | 3/6 = 0.5 | 2 × 1.86 | | 4 × 2.04 | | |
| Mg | 2/6 = 0.33 | 2 × 2.09 | | | | 4 × 2.19 |
| H(1) | | 1 × 1.01 | | 2 × 2.07 | | |
| H(2) | | 1 × 0.89<br>2 × 2.33 | | | | |

(b)

| Model | Valence sums at oxygen atom | | | | |
|---|---|---|---|---|---|
| | O(1) | O(2) | O(3) | O(4) | O(5) |
| 1 × 63.5% | 2.5−[a]<br>2[b] | 2 | 2+[a]<br>2 | 2 | 2 |
| 2 × 21.5% | 2.0−[c]<br>1.83+[d] | 2 | 2 | 2 | 1.83 |
| 3 × 15% | 2.0[e]<br>1.5[f] | 2 | 2 | 2 | 2 |

*Note.* Mg is occupying the U site in this simplified model.

[a] Bonded to H(1); hydrogen bonding to O(3) at 2.33 Å will transfer valence from O(1) to O(3).

[b] Bonded to Al(3).

[c] Bonded to H(2).

[d] Bonded to Mg and Al(3); hydrogen bonded at 2.33 Å to H(2).

[e] Bonded to two Al(2) and one Al(3).

[f] Bonded to two Al(2).

greatly when adjusted for substitution by other cations; this assumption is discussed later. The crucial experimental discovery in the present study is the presence of two types of H positions, H(1) and H(2), each represented by an *A* and *B* subsite. This changes the earlier discussions in which only one type of H position was assumed. Taken together with the tabulation of the pairs of adjacent cation sites which are too close for simultaneous occupancy (Table V), this leads to a unique domain model (Table IV).

Structural domain *2A* (population factor 0.115) contains H(2A), Mg(A), and Al(3A), but not Fe. Domain *2B* (population factor 0.10) is displaced by *c*/2 from domain *2A* and contains H(2B), Mg(B), and Al(3B); note that the deliberate choice of *A* and *B* for the atom designations in Table I facilitates the present description. The combined occupancy of 0.215 for domains *2A*

TABLE VII

ATOMIC NUMBER, IONIC RADII, AND NEUTRON SCATTERING LENGTH

| Ion | Z | Ionic Radius (Å) IV | VI[a] | Neutron S.L. ($\times 10^{-15}$ m)[b] |
|---|---|---|---|---|
| $H^1$ | 1 | — | — | −3.741 |
| $Li^1$ | 3 | 0.59 | 0.76 | −2.03 |
| $O^{-2}$ | 8 | — | — | 5.805 |
| $Mg^2$ | 12 | 0.57 | 0.72 | 5.375 |
| $Al^3$ | 13 | 0.39 | 0.53 | 3.449 |
| $Si^4$ | 14 | 0.26 | 0.40 | 4.149 |
| $Ti^4$ | 22 | 0.44 | 0.60 | −3.438 |
| $V^3$ | 23 | 0.50 | 0.64 | −0.382 |
| $Cr^3$ | 24 | 0.47 | 0.61 | 3.635 |
| $Mn^2$ | 25 | 0.69 | 0.83 | −3.73 |
| $Fe^2$ | 26 | 0.64 | 0.78 | 9.54 |
| $Fe^3$ | 26 | 0.35 | 0.49 | 9.54 |
| $Co^2$ | 27 | 0.60 | 0.74 | 2.53 |
| $Zn^2$ | 28 | 0.60 | 0.74 | 5.68 |

[a] Based on Ref. (*28*).
[b] Ref. (*26*).

and *2B* restricts the combined occupancy of the Fe site to a maximum of 0.785. Domains *1A* and *1B* utilize simultaneous occupancy of either H(1A) and Al(3A) or H(1B) and Al(3B) with Fe. To complete the cation assignments, domains *3A* (population factor 0.06) and *3B* (population factor 0.09) contain either Al(3A) or Al(3B) occupied simultaneously with Fe.

The combined domains give 78.5% occupancy of the Fe site and 100% occupancy of the *combined* Al(3A) and Al(3B) sites. All of the proposed occupancies for the sum of the combined domains *1A–3B* are within $2\sigma$ of the observed values, except for the Fe site whose observed population factor is 0.732(4) for occupancy only by Fe. Because Li, Mn, and Zn have smaller neutron scattering factors than Fe, their substitution in the Fe site can increase the effective occupancy to the proposed value for the combined domains. Hence, it is concluded that the occupancies for the domain model are generally consistent with the experimental evidence. For much of the later discussion it is sufficient to combine the six types of structural domains with monoclinic symmetry into three types with orthorhombic symmetry (Table IV(b)).

In addition to satisfying the diffraction evidence, the structural domains must satisfy the crystal-chemical requirements for a low internal energy. In an ionic model, the cations should be as far away as possible from each other, and the valence sums at the oxygen atoms should be near the formal negative charge of 2. Figures 2a, 2b, and 2c show projections onto the *ac* plane of the atomic positions from $y = 0$ to $\frac{1}{4}$. The kyanite slab is obtained from Si at $y = 0.166$, Al(1A,B) at 0.175, and Al(2) at 0.090. The (Fe, Al, Mg)–hydroxide layer contains Fe, Al(3A,B), and Mg(A,B) which all lie on the mirror plane at $y = 0$. For structural domain *1A*, a proton occupies each H(1A) site which lies between O(1B) and two O(3) about half-way between an occupied Fe site and an adjacent H(1A) site (Fig. 2a). When the Fe site is empty in structural domain *2A* (Fig. 2b), a proton occupies H(2A) which lies between O(1B) and O(1A). This position is fairly close to the center of a rectangle between the nearest Al(3A) and Mg(A) atoms. In structural domain *3A* (Fig. 2c), the Fe site is occupied but the H(1A) site is not; a possible explanation involving topochemical restrictions at domain boundaries is proposed later.

Table VI lists the coordination of oxygen atoms around the cation sites (a), and gives the formal valence sums at the five types of oxygen atoms for the three types of structural domains (b). The sums for O(2)–O(5) are 2 for each model, except for two oxygen atoms. One of the two O(3) atoms in domain 1 has a small excess because of hydrogen bonding at 2.33 Å, and O(5) in domain 2 has 1.83 valence units. Although the sums for O(1A) and O(1B) range from 1.5 to 2.5 for the different domains, such deviations of 0.5 from perfect local charge balance are present in other ionic structures (e.g., meli-

TABLE VIII

COMPARISON OF OBSERVED AND ESTIMATED POPULATIONS FOR X-RAY AND NEUTRON SCATTERING

| Site | Neutron Obs.[a] | Neutron Est.[b] | X-ray Obs.[c] | X-ray Est.[d] | Model composition |
|---|---|---|---|---|---|
| | | | (a) An extreme model with no Fe in U site | | |
| 8 Si | 0.990(6) | 0.993 | 0.986(6) | 0.997 | Si 7.67, Al 0.33 |
| 4 Fe | 0.732(4) | 0.747 | 0.76(1) | 0.770 | $Fe^2$ 3.00, Li 0.07, Mn 0.04, Zn 0.02, Co 0.01 |
| 8 Al(1) | 1.016(10) | 1.013 | 0.973(8) | 1.008 | Al 7.94, $Fe^3$ 0.06 |
| 8 Al(2) | 0.971(7) | 0.996 | 0.978(8) | 1.008 | Al 7.52, Mg 0.35, Ti 0.11, Cr 0.01, V 0.01 |
| 2 Al(3) | 0.98(2) | 0.997 | 0.96(2) | 1.006 | Al 1.88, Mg 0.09, Ti 0.03 |
| 2 U | 0.21(2) | 0.216 | 0.25(2) | 0.232 | Mg 0.41, Zn 0.02 |
| | | | (b) Same population, but with random ($Fe^{2+}$, Mg) | | |
| 4 Fe | 0.732(4) | 0.675 | 0.76(1) | 0.681 | $Fe^2$ 2.34, Mg 0.66, Li 0.07, Mn 0.04, Zn 0.02, Co 0.01. Total 3.14 atoms |
| 8 Al(2) | 0.971(7) | 1.032 | 0.978(8) | 1.049 | Al 7.52, $Fe^2$ 0.27, Mg 0.08, Ti 0.01, Cr 0.01, V 0.01 |
| 2 Al(3) | 0.98(2) | 1.035 | 0.96(2) | 1.048 | Al 1.88, $Fe^2$ 0.07, Mg 0.02, Ti 0.03 |
| 2 U | 0.21(2) | 0.403 | 0.25(2) | 0.356 | $Fe^2$ 0.32, Mg 0.09, Zn 0.02. Total 0.43 atoms |
| | | | (c) Transfer of 0.21 $Fe^{2+}$ from Fe site and 0.41 Mg from U site | | |
| 4 Fe | 0.732(4) | 0.752 | 0.76(1) | 0.765 | $Fe^{2+}$ 2.79, Mg 0.41, Li 0.07, Mn 0.04, Zn 0.02, Co 0.01. Total 3.34 atoms |
| 2 U | 0.21(2) | 0.197 | 0.25(2) | 0.230 | $Fe^{2+}$ 0.21, Zn 0.02. Total 0.23 atoms |

[a] Observed population and error (Table I, col. 5) for the ideal site occupancy of column 1; Mg is assumed for the U site.

[b] Estimate of the population factor from the model composition in the last column using simple linear proportion according to the scattering lengths in Table VII.

[c] Observed population and error for the ideal site occupancy of column 1, as proportioned from the X-ray data in Ref. (*6*) using the atomic number as a simple approximation to the atomic scattering factor.

[d] As for footnote *b*, but using the atomic number.

lite, Ref. (*29*); zoisite, Ref. (*30*)). In these structures, the deviations are compensated by variations of bond length. For staurolite, it is possible to obtain such compensation for each domain, but the details are too tedious to give here. Hence it is concluded that the three types of structural domains pass the energy test.

More subtle tests are provided by the Mössbauer spectrum for $^{57}Fe$, and the observed values of the anisotropic "temperature" factor. To a first approximation, the Mössbauer spectrum (Fig. 2 of Ref. (*6*)) can be fit with two doublets, an outer doublet with 77% intensity and an inner doublet with 23% intensity. The outer doublet can now be assigned on the basis of relative intensity to the Fe atoms in structural domain *1* and the inner doublet to those in domain *3*. Some minor complications are discussed later.

The "temperature" factors for the X-ray and neutron scattering of the Fe site are too large to represent just thermal motion, and the triple peaks (A, B, C) in the ($F_o$-$F_c$) synthesis for the X-ray diffraction data (Fig. 1 of Ref. (*6*)) demonstrated that there are at least three different centers-of-motion. Although the difference map for neutron diffraction (Fig. 1b) does not show a simple

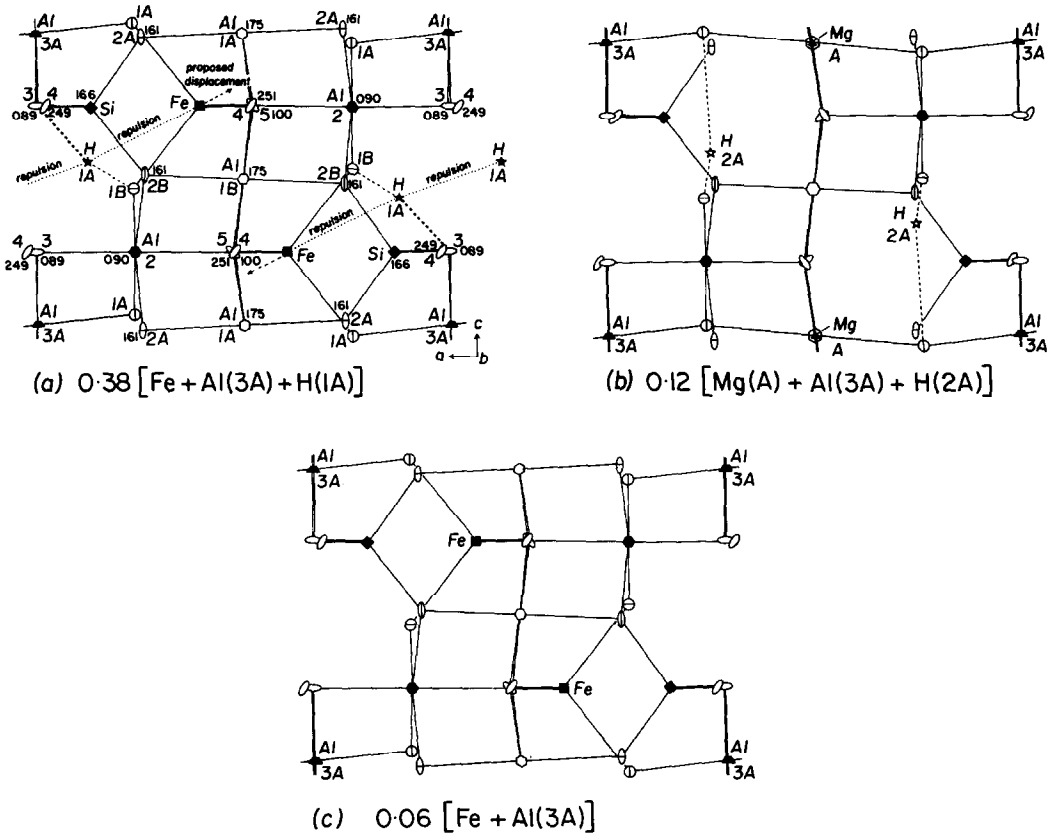


FIG. 2. Projections down the *b*-axis of a slice from $y = 0$ to 0.25 for three structural domains: (a) *1A*, (b) *2A*, and (c) *3A*. Each atom is shown with a distinctive symbol (cations, polygonal; oxygen, nonpolygonal). Atoms at $y \neq 0$ are given a three-figure number in thousandths. Metal–oxygen bonds are shown by continuous lines, and H–O linkages by dashed ones. Dotted lines in (a) show repulsion between H(1A) and Fe cations, and the arrows show the direction of the proposed displacements of the Fe sites.

triplet shape, it is generally consistent with the map for the X-ray data when account is taken of the random experimental error and the possible effects for a nonrandom distribution over the A–C sites of Li and Mn which have negative neutron scattering lengths. Peak A can be explained by displacement of Fe, etc., away from H(1A) in structural domain *1A* (Fig. 2a), B by a symmetrical displacement from H(1B) in domain *1B* (not shown), and C by lack of a displacement in the H-free domains *3A* and *3B*.

From the seven oxygen positions in Table I, it is O(1A), O(1B), and O(3) which have the largest values of $B_{iso}$ (see also Table II of Ref. (*6*)); these are the atoms which would be affected by the presence or absence of a proton in the H(1) and H(2) sites. Further interpretation is given later when the chemical substitutions have been considered.

To conclude this section, the concept of six structural domains satisfies the overall experimental data and the general crystal-chemical requirements. The next step is to

examine how the complex chemical composition can be interpreted in terms of this concept.

*Proposed Chemical Substitutions*

The present suggestions on the chemical substitutions for the six cation sites in the orthorhombic pseudostructure are obtained by simultaneous consideration of the bulk chemical composition (see Experimental), the observed and estimated population factors (Table VIII), and crystal-chemical considerations. The atomic number, ionic radii, and neutron scattering lengths of relevant species are given in Table VII.

Because the scattering factors for neutron diffraction are independent of Bragg angle $\theta$, the population factor for a site is linearly dependent on the atomic concentration multiplied by the scattering length. Thus the estimated value of 0.993 for 7.67 Al and 0.33 Si atoms in the Si site (Table VIII) is obtained from $[(7.67 \times 4.149) + (0.33 \times 3.449)]/(8.00 \times 4.149)$. For X-ray diffraction, the scattering factor is proportional to atomic number $Z$ at Bragg angle $\theta = 0$ for an unionized atom, but has a complex variation when ionization is considered. Furthermore, there is a variation with $\theta$, which interacts strongly with the temperature factor in least-squares refinements. For simplicity, the population factors for X-ray scattering are proportioned to $Z$, but it must be emphasized that the listed error does not cover any systematic uncertainty.

The following sequence is followed. First, the eight Si sites are filled with 7.668 Si and 0.332 Al to satisfy the observed population factors and the widespread evidence for Si,Al substitution in tetrahedral sites (e.g., feldspar, pyroxene). Second, the proposed 78.5% occupancy of the fourfold Fe site requires 3.14 atoms compared to the 3.002 $Fe^{2+}$ atoms in the bulk analysis. From the crystal-chemical viewpoint (Table VII), $Li^{1+}$, $Mn^{2+}$, $Zn^{2+}$, $Co^{2+}$, and $Mg^{2+}$ are possible substituents. From the experimental viewpoint, the apparent population factor for X-ray scattering is higher than for neutron scattering; this can be achieved especially well by substitution of Li (low $Z$; negative scattering length). Hence the 0.067 Li is placed in the Fe site, and the remaining positions are filled with 0.042 Mn (negative scattering length), 0.007 Co, and 0.022 Zn. The latter three assignments are convenient mathematically, and the latter two species would not be needed if the Fe analysis is too low by only 1%! Assignment of Li and Zn to the Fe site is consistent with (*15*). Magnesium is not assigned to the Fe site because it can be assigned conveniently to the U and Al sites. However, it would be possible to exchange some $Fe^{2+}$ with $Mg^{2+}$ without serious violation of the experimental constraints. Third, Mg can be readily assigned to the U sites because of its appropriate ratio of neutron to X-ray scattering. For convenience, the remaining 0.025 Zn atoms are placed in this site together with 0.405 Mg to match the $2 \times 0.215$ atoms for structural domain *2* (Table IV(b)). These assignments of Mg and Zn are satisfactory from the crystal-chemical viewpoint. Fourth, the assignment of the remaining atoms (Al 17.354, Ti 0.138, Cr 0.011, V 0.009, $Fe^{3+}$ 0.061, Mg 0.441; total 18.014) to the eight Al(1), eight Al(2), and two Al(3) sites is difficult and uncertain because the changes in the estimated population factors from transfer of the minor elements are small except for Al(3). Because Mg has a larger scattering length (5.375) than Al (3.449), and Ti has a negative scattering length (−3.438), it seems best to couple Mg and Ti in order to explain the near equality of the estimated populations of the Al sites. The high scattering length of Fe (9.54) favors placement of the $Fe^{3+}$ in Al(1). The proposed assignments (Al(1), Al 7.939, $Fe^{3+}$ 0.061; Al(2), Al 7.517, Mg 0.353, Ti 0.110, V 0.009, Cr 0.011; Al(3), Al 1.884, Mg 0.088, Ti 0.028) give estimated neutron scattering lengths in the same numerical se-

quence as the observed ones, but it must be fully recognized that other possible distributions are compatible with the experimental uncertainties.

To conclude this section, it is possible to make some *minor* adjustments in the above distributions (especially for Mg and Zn), and indeed slight improvements can be obtained by some changes. The important conclusion at this stage is the likelihood that at least most of the $Fe^2$, and at least some of the Li, Mg, and Ti are present as in Table VIII. This established a reliable basis for decisions on what further measurements will lead to a more complete answer.

Table VIII illustrates the sensitivity of the structural assignments. Randomization of the Mg and $Fe^{2+}$ atoms (b) over the sites in the preferred simple model (a) leads to major problems for the U site. Transfer of 0.21 $Fe^{2+}$ from the Fe site to the U one, and of 0.41 Mg in the reverse direction gives a satisfactory fit between observed and estimated population factors. Furthermore, the X-ray and neutron scattering factors for Mg and $Li_{0.5}Fe_{0.5}$ are not greatly different. A third type of tolerance involves the $Fe^{3+}/Fe^{2+}$ ratio. It is possible to double the value assumed in the simple model without serious problems in matching the observed and calculated population factors. However, the simple model does give a reasonable fit to all the data, and is preferred for its simplicity.

The remainder of the discussion considers specific chemical and structural features.

*Iron*

The present estimate that 2% of the iron is trivalent is not rigorously justified. Mössbauer spectra for staurolites from various localities consist principally of two doublets (*6, 16–20*) and it would be difficult to unambiguously detect peaks for a small fraction of $Fe^{3+}$ in octahedral coordination; however, 2–3% ferric iron was inferred for a small doublet of unspecified parameters (*19*) (see also (*16*) and Ref. (*32*) received after completion of the manuscript). Large fractions of $Fe^{3+}$ in wet chemical analyses can be largely discounted, probably because oxidation occurred during dissolution. In the preceding section, the assumption of 2% $Fe^{3+}$ resulted in a total of 18.014 atoms for the 18 Al sites. This excess of 0.014 atoms would decrease for a higher amount of $Fe^{3+}$, but it must be emphasized that a plausible error of 1% in the bulk Al content rules out any attempt to use stoichiometry as a test of the $Fe^{3+}$ content.

The assignment of both doublets in the Mössbauer spectrum to tetrahedral $Fe^{2+}$ agrees with the suggestion in (*16*). For the stronger doublet of a low-Fe staurolite from Brittany, now assigned to Fe in structural domain *1*, it was concluded (*19*) from single-crystal Mössbauer spectra that the principal axis of the electrostatic field gradient lies in (001) at ~55° from *c*. Because the repulsive forces between $Fe^{2+}$ and H(1) are in the (010) plane at 63° to *c*, there is no obvious explanation of this conclusion. Further single-crystal spectra are needed, especially for a Pizzo Forno staurolite. The magnetic ordering below 7 K (*19, 20*) is attributed to spin–spin interaction between pairs of adjacent $Fe^{2+}$ atoms separated by 3.3 Å in the $y = 0$ plane.

The broadness of the inner doublet for $Fe^{2+}$ in domain *3* is compatible with the overlap of several components that would result from the complex cation substitution in Table VIII. In particular, the electrostatic field gradient at the Fe site (Fig. 2c) would change in response to substitution of either $Mg^2$ or $Ti^4$ in the adjacent sites, Al(3A) at 3.5 Å and two Al(2) at 3.3 Å.

If the reported intensity ratio of 77 : 23 (= 3.3) for the outer and inner doublets (*6*) were truly representative of the partitioning of Fe between structural domains *1* and *3*, there would be a minor problem. Even if all the Fe sites of domain *3* were occupied by

Fe, and all the Li, Mn, Zn, and Co were in the Fe sites of domain *1*, the resulting minimum ratio of Fe (domain *1*)/Fe (domain *3*) would be only 4.0. However, since the intensity ratio changes with temperature of measurement from 82.5 : 17.5 (= 4.7) at 298 K to 86.9 : 13.1 (= 6.6) at 45 K for a Minas Gerais staurolite (*20*), it is necessary to obtain a detailed theoretical understanding of the physical factors which control the intensities of the Mössbauer resonances of staurolite before attempting to quantify the relation between the observed intensities and the chemical features of the domain model in Table IV. Furthermore, the quadrupole splitting for tetrahedral high-spin $Fe^{2+}$ depends theoretically on axial distortion and temperature (*33*), and a detailed analysis of new Mössbauer absorption data for the present specimen is needed.

The above discussion must be modified if some of the $Fe^{2+}$ is in the U site. An additional set of Mössbauer resonances would be needed but they could be unresolved from the other resonances. For the future, it is necessary to understand how the site distribution and population factors of both $Fe^{2+}$ and $Fe^{3+}$ are related to the number of H atoms; in particular, the exclusion relations among the Fe, U, and H(2) sites (Table V) should be important in controlling speculations.

*Hydrogen*

The H(1A) and H(1B) positions correspond to the two principal proton nuclear-magnetic resonances reported in (*13*): note that the P(1A) and P(1B) labels in (*13*) have been switched to H(1B) and H(1A) to match the assignments of A and B in Table IV. The principal eigenvectors were deduced to lie at $\cos^{-1}(-0.42) = 114.8°$ and $\cos^{-1}(0.40) = 66.4°$ to the *c*-axis in (010). These values match well with those for the H(1A)–Fe and H(1B)–Fe vectors in the present structure (117.2 and 62.9°, respectively) as suggested in (*13*). Actually each H(1) lies almost midway between another H(1) and an Fe (Fig. 2a). The H(1)–H(1) vector lies at 108.7° and 71.5° to *c* for the A and B subsites, and it is likely that each proton interacts with its adjacent proton as well as the Fe atom.

A third resonance (probably an overlapping pair) was unassigned in (*13*). Its weak and broad nature is not inconsistent with the weak and elongated neutron-scattering peaks for H(2A) and H(2B) in Fig. 1a. The poorly determined angle of $\cos^{-1}0.11 = 83.7°$ to the *c*-axis in (010) is not inconsistent with the angles of 70.0° and 70.9° for the vectors between adjacent pairs of H(2A) and H(2B) in Fig. 2b when account is taken of contributions to the electrostatic field from the various cations, including those in Al(3) and Mg sites.

Because of the structural disorder, there must be some changes in the positions of O(1) and O(3) depending on the occupancy of the nearby sites. Such changes, however, will be too small to modify the general coordinations of the H atoms in Figs. 2a and 2b. Thus the H(1) protons are strongly bonded to O(1) at ~1.0 Å, and show bifurcated hydrogen bonding to two O(3) at ~2.0 Å; in contrast, the H(2) protons are bonded to two O(1), one at ~0.9 Å and the other at ~2.3 Å. Because there are more H(1) than H(2) protons, the observed distances to H(1) should be closer to the true ones than for H(2).

For the two-dimensional study in (*13*), the H(2) positions would be hidden by one of the three lobes for Fe in the difference-Fourier projection. However, there is no obvious explanation for the absence of the H(2) positions in the three-dimensional neutron-diffraction study of a staurolite from the St. Gotthard region (*14*). This study was made at 77 K, which is bracketed by the X-ray study at room temperature (*6*) and the neutron-diffraction study at 13 K of the present St. Gotthard specimen. For the present model of structural domains, occu-

pancy of the H(2) sites is coupled with occupancy of Mg sites, which were found to be populated in (*14*). A difference-Fourier synthesis of the 77 K data should be examined to test whether the present structural model applies only to the present specimen from St. Gotthard at 13 K.

*Titanium*

Crucial to a satisfactory crystal-chemical model of staurolite is whether Ti is in tetrahedral or octahedral coordination. This should be resolved by an EXAFS study now in progress. For the present, it does not seem necessary to accept the suggestion in (*23*) that the $Fe^{2+}$–$Ti^{4+}$ charge transfer, which is necessary for explanation of the color of staurolite, implies that both cations are in tetrahedral sites. Assignment of $Ti^{4+}$ to the octahedral Al(2) or Al(3) sites (Table VIII) would bring it as close to $Fe^{2+}$ in the Fe site (3.26 and 3.32 Å, respectively) as for residence in an Fe site (3.27 Å).

*Cobalt*

A paper on the crystal structure of a cobaltoan staurolite (*34*) was received after completion of this work. Because Co has similar X-ray scattering to Fe, the new data can be interpreted according to the present model. It is important to obtain neutron diffraction data for this specimen to take advantage of the difference in X-ray and neutron scattering.

*Atomic Displacements and Chemical Substitutions*

The unusually high values of $B_{iso}$ for Fe, O(1A), O(1B), and O(3) were explained earlier in terms of atomic displacements related to the presence or absence of the H(1) and H(2) protons. For the fully occupied sites Si, Al(1), Al(2), O(2), O(4), and O(5) the values of $B_{iso}$ (Table I) are comparable to but rather larger than those for *ordered* silicate structures at ~10 K (e.g., low albite at 13 K, Al and Si 0.19–0.20, O 0.29–0.42 $Å^2$ (*35*)). In addition to the zero-point motion, it seems likely that all atoms in staurolite are affected to some degree by displacements related to atomic substitution. Examination of the anisotropic temperature factors (Table II) shows that the root-mean-square displacement ($u_{ij}$) is larger in the *c* direction than the *a* and *b* ones, except for H(2A) and H(2B) which have a particularly large displacement along *a* (cf. Fig. 1a). The overall anisotropy might be ascribed to the structural disorder between the *A* and *B* subunits which causes the monoclinic deviation from orthorhombic symmetry, or by effects caused by substitutional disorder.

*Interatomic Distances and Angles*

When account is taken of the likely chemical substituents, and of the averaging for occupied and unoccupied fractions of partly occupied sites, all the distances and angles in Table III are reasonable. In particular, the H–O distances are affected at the 0.0- to 0.1-Å level by the substitutional disorder. For the Fe site, there are significant displacements from the centroid (Fig. 1 of (*6*)) of about 0.2–0.3 Å, and the high precision (~0.001 Å) of the Fe–O distance applies only to the centroids and not to the distances in the individual domains.

*Relation between the Structural Domains and the Monoclinic Symmetry*

Because non-Bragg and superstructure diffractions have not been observed for staurolite, there is apparently no long-range order or near-regular short-range order. Nevertheless it is necessary to consider how the six types of structural domains can be fitted together in one coherent crystal which is assumed to have a full complement of Si, Al(1A,B), Al(2), and O atoms. If there are topochemical and topological incompatibilities, it will be necessary to consider the structural changes required at domain boundaries.

Consider first the Al(3A) and Al(3B) at-

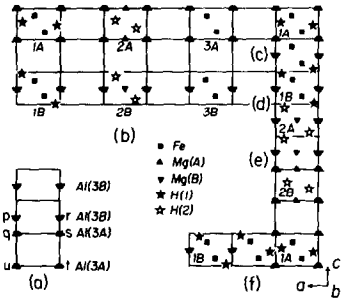


FIG. 3. Diagrams illustrating some topochemical factors at the boundaries of structural domains. A section at $y = 0$ is shown through an $8 \times 7$ array of unit cells. The cation symbols are the same as in Fig. 2. Diagram (a) shows a possible type of boundary between Al(3A) atoms at *qsut* and Al(3B) atoms at *pr*. Diagram (b) shows the cation positions for single unit cells of the six types of structural domains 1A–3B. Some possible boundaries between domains of type 1 and 2 are shown at (c)–(f).

oms which have been assumed so far to have a combined population of 2, which equals 50% of the twofold Al(3A) and twofold Al(3B) sites. For random occupancy, some of the adjacent Al(3A) and Al(3B) sites in the $y = 0$ plane must be occupied (Fig. 3a; sites *p,q* and *r,s*). Since these sites are only 2.83 Å apart, there is a significant contribution to the internal energy from an ionic model, which would favor an ordered monoclinic single crystal over a disordered orthorhombic crystal. The possibility of vacant Al(3) sites at antiphase boundaries should be considered, but this might involve an even larger contribution to the internal energy because of the low valence sum at oxygen atom O(3).

Consider next the relationship between the cations and protons of structural domains *1A–3B* (Fig. 3b). When each structural domain is fully ordered with each unit cell identical to its neighbors, the cations are nicely distributed in positions with low electrostatic energy, as described earlier. At boundaries between some, but not all, domains, it is not possible to retain all the cation positions. Thus at (c), the boundary cell between the *1A* and *1B* domains lacks a proton and has adjacent Al(3A) and Al(3B). Domains *1B* and *2A* are compatible at (d), but domains *2A* and *2B* are not compatible at (e) where the boundary cell has adjacent Al(3A), Al(3B), Mg(A), and Mg(B). At (f), domains *1A* and *1B* are separated by a unit cell with a full complement of Fe, H(1B), and Al(3B), but it lacks monoclinic symmetry elements. No attempt was made to enumerate all possible examples, but it is obvious that the structural domains can be fitted together in many ways, and that only some of them are topochemically compatible for a low-energy ensemble. The H-free domains of types 3A and 3B might provide a low-energy boundary between H-bearing domains. If so, the present structural model will require modification for the rare natural staurolites with more than 4H per unit cell (*15*).

To conclude this section, it is necessary to point out that the apparently good fit between structural models and diffraction data for the simple models of *isolated* structural domains implies that most atoms belong to a well-ordered domain, and that boundary misfits should be relatively rare.

### *Coupled Chemical Substitutions*

It is necessary to consider what is the relative spatial distribution of those minor chemical substituents (Table VIII) which do not immediately fit into the simple structural domains of Table IV. To simply the problem, consider only the cations with a charge different from that of the prototype, namely $Al^3$ in the Si site, $Li^1$ in the $Fe^2$ site, and $Mg^2$ and $Ti^4$ in the Al sites. It is obvious from the information in Table VI that coupled substitutions of the minor elements could give a lower electrostatic energy than random substitutions. Thus coupled substitutions of $Al^3$ for $Si^4$, $Li^1$ for $Fe^2$, and 2 $Ti^4$ for 2 $Al^{3+}$ would preserve a local charge balance. Absence or presence of H is also important. No attempt was made to list all

the likely combinations, and further discussion is deferred to another paper. See Ref. (*36*) for new data on Li in staurolite and a discussion of coupled substitutions.

## Concluding Remarks

The following experiments are suggested to test and extend the above structural and chemical models: (a) EXAFS measurements of Ti and other transition elements to determine the local coordination, (b) X-ray and neutron diffraction analyses for staurolites which are rich in Li, Zn, Mg, and H (e.g., specimens 6–3, 117189, EH-6, 77-55C, 71-60E of (*15*)), (c) neutron diffraction analysis of the present specimen at room temperature to determine the effect of temperature on the atomic positions and displacements, particularly of the H atoms—this is desirable for rigorous interpretation of the changes of intensities and quadrupole splitting of the resonances in the Mössbauer spectrum (*19, 20*), (d) electron-optical study of the present specimen to extend the study in (*8*), (3) systematic study of the Mössbauer and optical absorption spectra of the specimens chosen for (b), and (f) systematic synthesis of staurolites from bulk compositions compatible with the present structural and chemical concepts, as already done for an Fe–Co series (*37*). From the theoretical viewpoint, much more work is needed to explore the topochemical properties of the present models, and to make estimates of the configurational entropy. The significance of the present crystal-structure study for the occurrence of staurolite in rocks will be discussed elsewhere.

Finally, it is interesting from a historical viewpoint to examine the many papers in the bibliography for the development of both correct and incorrect ideas on the chemical and physical nature of staurolite. The present study owes a great debt to the ideas of the earlier workers, who did not have access to the wealth of information available here.

## Acknowledgments

We thank J. Henriques for valuable technical assistance. K.S. thanks the Swedish Natural Sciences Research Council for financial support. J.V.S. thanks M. J. Holdaway for the supply of preprints which were critical to the chemical interpretation, N. Weber for preparing the manuscript, and the National Science Foundation for funding the Materials Research Laboratory at Chicago (DMR 82-16892). We thank the following for reviews: M. J. Holdaway and P. H. Ribbe.

## References

1. P. H. Ribbe, "Reviews in Mineralogy 5" (P. H. Ribbe, Ed.), Mineral. Soc. America, Washington (1982).
2. J. D. H. Donnay and G. Donnay, *Tschermaks Mineral Mitt.* **31,** 1 (1983).
3. I. Náray-Szabó, *Z. Kristallogr.* **71,** 103 (1929).
4. V. J. Hurst, J. D. H. Donnay, and G. Donnay, *Mineral. Mag.* **31,** 145 (1956).
5. I. Náray-Szabó, and K. Sasvari, *Acta Crystallogr.* **11,** 862 (1958).
6. J. V. Smith, *Amer. Mineral.* **53,** 1139 (1968).
7. K. Hanisch, *Neues Jahrb. Mineral. Monatsh.*, 362 (1966).
8. J. J. Fitzpatrick, Ph.D. thesis, University of California, Berkeley (1976).
9. A. Juurinen, *Ann. Acad. Sci. Fenn., Ser. A3* **47,** 1 (1976).
10. D. T. Griffen, T. C. Gosney, and W. R. Phillips, *Amer. Mineral.* **67,** 292 (1982).
11. S. W. Lonker, *Contrib. Mineral. Petrol.* **84,** 36 (1983).
12. M. J. Holdaway, B. L. Dutrow, J. Borthwick, P. Shore, and R. S. Harmon, *Amer. Mineral.* **71,** 1135 (1986).
13. Y. Takéuchi, N. Aikawa, and T. Yamoto, *Z. Kristallogr.* **136,** 1 (1972).
14. T. Tagai and W. Joswig, *Neues Jahrb. Mineral. Monatsh.*, 97 (1985).
15. M. J. Holdaway, B. L. Dutrow, and P. Shore, *Amer. Mineral.* **71,** 1142 (1986).
16. E. Dowty, *Earth Planet. Sci. Lett.* **15,** 72 (1972).
17. B. L. Dickson and G. Smith, *Canad. Mineral.* **14,** 206 (1976).
18. G. M. Bancroft, A. G. Maddock, and R. G. Burns, *Geochim. Cosmochim. Acta* **31,** 2219 (1976).
19. J. R. Regnard, *J. Phys. Colloq.* **37,** 797 (1976).
20. R. B. Scorzelli, E. Baggio-Saitovitsch, and J. Dannon, *J. Phys. Colloq.* **37,** 801 (1976).

*21.* N. DZHEMAI, *Zap. Vses. Mineral. Ova* **107,** 205 (1978).
*22.* G. A. WAYCHUNAS, M. J. APTED, AND E. BROWN, JR., *Phys. Chem. Miner.* **10,** 1 (1983).
*23.* C. M. WARD, *Amer. Mineral.* **69,** 541 (1984).
*24.* K. STÅHL, Å KVICK, AND J. V. SMITH, *Eos* **66,** 400 (1985).
*25.* P. J. BECKER AND P. COPPENS, *Acta Crystallogr., Sect. A* **30,** 129 (1974).
*26.* L. KOESTER, H. RAUCH, M. HERKENS, AND K. SCHROEDER, Kernforchungsanlage Report JUL-1755 (1981).
*27.* J.-O. LUNDGREN, Report No. UUIC-B13-4-05, University of Uppsala, Sweden (1983).
*28.* R. D. SHANNON, *Acta Crystallogr., Sect. A* **32,** 751 (1976).
*29.* J. V. SMITH, *Amer. Mineral.* **38,** 643 (1953).
*30.* J. V. SMITH, J. J. PLUTH, J. W. RICHARDSON, JR., AND Å KVICK, *Z. Kristallogr.,* in press.
*31.* K. STÅHL, *Acta Crystallogr., Sect. B* **39,** 612 (1983).
*32.* H. V. VARMA AND J. VARMA *Phys. Status Solidi* (9) **97,** 275 (1986).
*33.* T. C. GIBB, *J. Chem. Soc. A,* 1439 (1968).
*34.* K. N. BRINGHURST AND D. T. GRIFFEN, *Amer. Mineral.* **71,** 1466 (1986).
*35.* J. V. SMITH, G. ARTIOLI, AND Å KVICK, *Amer. Mineral.* **71,** 727 (1986).
*36.* B. L. DUTROW, M. J. HOLDAWAY, AND R. W. HINTON, *Contrib. Mineral. Petrol.* **94,** 496 (1986).
*37.* L. V. PHILLIPS AND D. T. GRIFFEN, *Amer. Mineral.* **71,** 1463 (1986).